IEEE Access
Multidisciplinary | Rapid Review | Open Access Journal

Received February 6, 2021, accepted March 29, 2021, date of publication April 1, 2021, date of current version April 14, 2021.

Digital Object Identifier 10.1109/ACCESS.2021.3070479

Research on Seismic Input Method of Layered Ground Foundation

ZHONGHUI BI[1,2], BINGHUI CUI[3], AND YAFEI ZHAI[1,2]
[1]State Key Laboratory of Hydrology-Water Resources and Hydraulic Engineering, Hohai University, Nanjing 210024, China
[2]College of Water Conservancy and Hydropower Engineering, Hohai University, Nanjing 210024, China
[3]College of Civil and Transportation Engineering, Hohai University, Nanjing 210024, China

Corresponding author: Binghui Cui (bhcui19@hhu.edu.cn)

This work was supported in part by the National Key Research and Development Program under Grant 2017YFC0404903, in part by the National Natural Science Foundation of China under Grant 51709090, and in part by the Natural Science Foundation of Jiangsu Province under Grant BK20170884.

ABSTRACT The seismic input of layered foundation is an essential part of seismic analysis of structure-foundation system. Most of the traditional seismic input methods only consider the first reflection process of seismic waves at the interface of different media, ignoring the subsequent reflection and refraction propagation process, which can not truly reflect the wave propagation process in the layered foundation. This paper proposes a new seismic input method for layered foundation, considering all reflected and refracted waves. Firstly, the viscous-spring artificial boundary model of the layered foundation is established, which can simulate the absorption of scattered waves and the elastic recovery capacity of semi-infinite foundation at the same time. Then, based on the wave mechanics theory, the equivalent nodal force calculation formula is derived to realize the vibration input of layered ground. Finally, the calculation results of the layered foundation and two-way surge tower engineering are verified. The results show that: compared to the traditional input method, the method proposed in this paper has a significant influence on the seismic response of layered foundation, and the method in this paper can better meet the accuracy requirements of engineering earthquake resistance, which provides an effective and practical calculation method for seismic analysis of layered foundation structure.

INDEX TERMS Layered foundation, reflection, refraction, equivalent nodal force, viscous-spring artificial boundary.

I. INTRODUCTION

In the past few decades, there have been hundreds of severe earthquake disasters globally, which have caused significant losses to people's lives and properties. Simultaneously, buildings are faced with complex site foundation conditions, which puts forward higher requirements for seismic design and safety evaluation [1].

Many scholars have researched the dynamic interaction between building and foundation [2]–[5]. The radiation damping effect caused by the propagation of seismic waves in the infinite foundation is the key to this problem. Among the wave propagation simulation methods, the finite difference method and the finite element method are the two most essential simulation methods [6], [7]. Considering the reflection of the wave propagating to the near-field boundary, it is necessary to apply a method of artificial absorbing boundary on the near-field truncated boundary to simulate the radiation damping effect of infinite foundation on the seismic wave [8], [9]. Deeks *et al.* [10] proposed a viscous-spring artificial boundary model that can simultaneously stimulate the absorption of scattered waves and semi-infinite elastic foundation recovery capacity. This method is easy to implement and has been widely used. Liu *et al.* [11] and others have derived a model of the three-dimensional viscous-spring artificial boundary in the time domain and simplified the realization of wave input through equivalent nodal force. Du *et al.* [12] and others extended that it can be used for cylindrical elastic wave radiation. Chen *et al.* [13] applied the three-dimensional viscous-spring artificial boundary in the time domain to the arch dam's seismic input. They explored the non-linear dynamic response law of the dam when seismic

The associate editor coordinating the review of this manuscript and approving it for publication was Zheng H. Zhu.

wave incidence occurred. The above research is based on a homogeneous foundation, but in practical engineering, the layer is often distributed in a complicated way in the foundation. Compared to that in the semi-infinite homogeneous foundation, the wave propagation in the semi-infinite layered foundation is more complex, mainly reflected in that there are both traveling waves with the energy dissipating to infinity fast fading waves with the energy dissipating in the near-field [14].

Some scholars studied the input method of this kind of layered ground motion input and have put forward some effective numerical simulation methods. Wolf *et al.* [15] proposed the scaled boundary finite element method, which only needs to discretize the computational domain's boundary. The semi-infinite boundary wave problem, it does not need the fundamental solution to satisfy the radiation damping boundary condition in wave propagation. Nakamura *et al.* [16] proposed a dynamic stiffness calculation method for the horizontal multi-layer rigid foundation, which transforms the complex stiffness into a time domain. Birk *et al.* [17] used the high-frequency asymptotic series method to solve the three-dimensional layered foundation's dynamic stiffness. The calculation is relatively heavy, and it does not perform well inaccuracy. Based on the propagation principle of seismic waves in a layered elastic medium, Fan *et al.* [18] proposed a fast time -domain algorithm for calculating layered foundation sites' seismic response improved the calculation efficiency. Liang *et al.* [19] used the two-dimensional SH-wave model of the shear wall on the rigid semi-circular foundation in layered half-space and used the indirect boundary element method to study the influence of dynamic characteristics of layered soil on soil-structure interaction in the frequency domain. Based on the proportional boundary finite element method, Han *et al.* [20] proposed a new coordinate transformation method to solve the dynamic stiffness of layered foundation and the Green function numerical algorithm for calculating the dynamic stiffness of layered foundation successively. The improved method overcomes traditional methods' limitation and improves the calculation accuracy and efficiency of dynamic stiffness of layered foundation. Chen *et al.* [21] used the proportional boundary finite element method to simulate the wave input problem in the layered foundation. The integral convolution algorithm is involved in the dynamic solution. Premramate *et al.* [22] constructed a high-order double asymptotic transmission boundary model based on the asymptotic solution of dynamic stiffness continued fraction, which achieves good numerical stability and can obtain accurate dynamic stiffness fast. Gao *et al.* [23] established a simplified high-order double asymptotic transmission boundary model based on the decoupled scalar wave equation. They used the model to simulate the propagation of elastic waves in the layered foundation. Liu *et al.* [24] applied the high-order double asymptotic transmission boundary model to the time-domain analysis of the interaction between the underground station and layered soil. Yin *et al.* [25] proposed a viscous-spring artificial boundary model considering the direct reflection of the wave on the top of the layered foundation and applied it to the seismic analysis of gravity dams on the layered foundation. Sotoudeh *et al.* [26] carried out a dynamic study on the layered foundation-gravity dam- reservoir water system based on the regional reduction method, which shows that the layered foundation and homogeneous foundation have a significant influence on the dynamic response of the dam.

In this paper, based on the previous research results, a new seismic input method for the layered foundation is proposed, combining the viscous-spring artificial boundary theory and the wave propagation law in layered soil. The method considers the refraction and reflection characteristics of elastic waves in different layered media and simulates the radiation damping effect of infinite foundation on the seismic wave. The fluctuation input is realized through programming and verified by two examples.

II. VISCOUS-SPRING ARTIFICIAL BOUNDARY MODEL OF LAYERED FOUNDATION

When the numerical method simulates the interaction between structure and foundation, considering that the natural foundation is a semi-infinite region, the numerical simulation calculation is enormous. It is necessary to intercept the finite near-field foundation from the natural foundation for calculation, and apply the artificial boundary model on the foundation's truncated boundaries to simulate the radiation damping effect of infinite foundation on the seismic wave [27], [28].

Fig. 1 shows a near-field layered foundation model with L layers. Seismic waves are vertically incident from the bottom of the model, and the viscous-spring artificial boundary model is applied on the near-field truncated boundary.

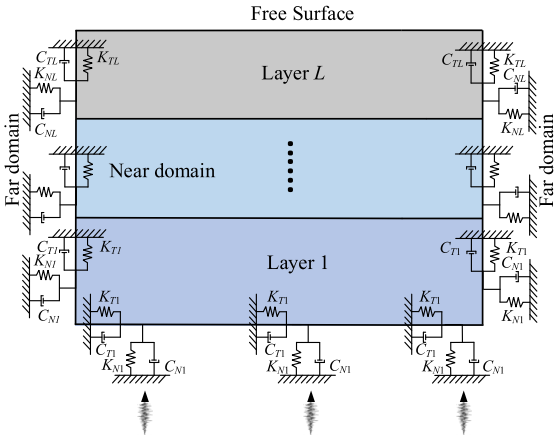

FIGURE 1. Model of layered half space foundation with the seismic wave incident.

The viscous-spring artificial boundary model can be simulated by parallel spring-damper elements with the continuous spatial distribution. The parameters of spring and damper applied to the three-dimensional viscous-spring

artificial boundary model are as follows:

$$\begin{cases} K_{NL} = \alpha_N \dfrac{G_L}{r}, C_{NL} = \rho_L V_{PL} \\ K_{TL} = \alpha_T \dfrac{G_L}{r}, C_{TL} = \rho_L V_{SL} \end{cases} \tag{1}$$

where K_{NL} and K_{TL} are the normal stiffness and tangential stiffness of the L layer spring, respectively; C_{NL} and C_{TL} are the normal damping and tangential damping of the L layer damper, respectively; α_N and α_T are the normal and tangential viscous-spring artificial boundary modification parameters, taken as $\alpha_N = 1.33$, $\alpha_T = 0.67$ [11]; r is the distance from the wave source to the artificial boundary point; G_L is the shear modulus of the L layer soil; ρ_L is the density of the L layer soil; V_{PL} and V_{SL} are, respectively, the P-wave velocity and S-wave velocity of the L layer soil, which can be calculated by (2)

$$\begin{cases} V_{PL} = \sqrt{\dfrac{\lambda_L + 2G_L}{\rho_L}} \\ V_{SL} = \sqrt{\dfrac{G_L}{\rho_L}} \end{cases} \tag{2}$$

where λ_L is the Lame constant of the L layer soil.

$$\begin{cases} K_{bNL} = \alpha_N \dfrac{G_L}{r} S_{bL}, C_{bNL} = \rho_L V_{PL} S_{bL} \\ K_{bTL} = \alpha_T \dfrac{G_L}{r} S_{bL}, C_{bTL} = \rho_L V_{SL} S_{bL} \end{cases} \tag{3}$$

where K_{bNL} and K_{bTL} are the normal spring stiffness and tangential stiffness of node b in the L layer, respectively; C_{bNL} and C_{bTL} are the dampers normal damping and tangential damping of node b in the L layer, respectively; S_{bL} is the influence area of node b in the L layer, as shown in Fig. 2.

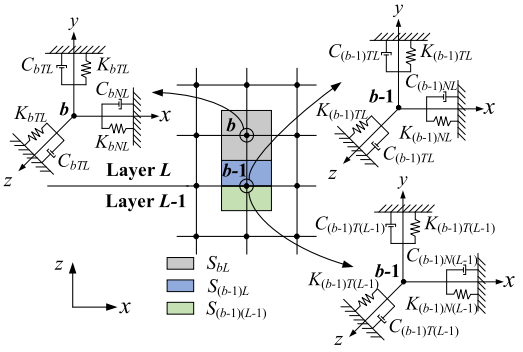

FIGURE 2. Schematic diagram of the spring damping element of 3D finite element model.

III. WAVE MOTION INPUT METHOD FOR LAYERED FOUNDATION

A. PROPAGATION CHARACTERISTICS OF ELASTIC WAVE

When the elastic wave enters into another medium from one medium, it will refract and reflect at the interface between the two media. The reflected wave will propagate downward in the incident medium, while the refracted wave will propagate upward in the above medium [29]. The P-wave and S-wave wave is incident perpendicularly to the interface of different media, and the wave pattern of the reflected wave and refracted wave do not change, as shown in Figure. 3. In Fig. 3, the blue arrow indicates the wave's propagation direction, and the red arrow indicates the vibration direction of the wave. A represents the wave amplitude, and the subscripts i, r, and t represent the incident wave, reflected wave, and refracted wave, respectively; the subscripts P and S represent the P-wave and S-wave, respectively; the subscript L, $(L-1)$ represents the L layer and $(L-1)$ layer, respectively.

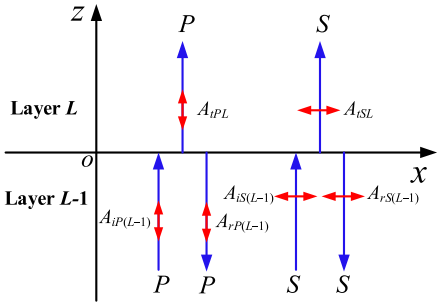

FIGURE 3. Incidence, reflection, and refraction of P-wave and S-wave at the interface.

It is assumed that the impedance ratios of S-wave and P-wave in layer L and layer $(L-1)$ are z_S and z_P, respectively:

$$\begin{cases} z_S = \dfrac{\rho_L V_{SL}}{\rho_{(L-1)} V_{S(L-1)}} \\ z_P = \dfrac{\rho_L V_{PL}}{\rho_{(L-1)} V_{P(L-1)}} \end{cases} \tag{4}$$

where $\rho_{(L-1)}$ is the density of the $L-1$ layer soil; $V_{P(L-1)}$ and $V_{S(L-1)}$ are, respectively, the P-wave velocity and S-wave velocity of the $L-1$ layer soil.

When P-wave and S-wave are vertically incident into layer L from layer $L-1$, the amplitude ratio of the reflected wave to incident wave in layer $L-1$ is $\alpha_{rP(L-1)L}$ and $\alpha_{rS(L-1)L}$, respectively, and the calculation formula is shown in (5) and (6); The amplitude ratio of refraction wave to incident wave in layer L is $\alpha_{tP(L-1)L}$ and $\alpha_{tS(L-1)L}$, respectively, and the calculation formula is shown in (7) and (8); When P-wave and S-wave are vertically incident into the $L-1$ layer from the L layer, the amplitude ratio of the reflected wave to the incident wave in the $L-1$ layer is $\alpha_{rPL(L-1)}$ and $\alpha_{rSL(L-1)}$, and the calculation formula is shown in (9) and (10); The amplitude ratio of the refracted wave to the incident wave in the $L-1$ layer is $\alpha_{tPL(L-1)}$ and $\alpha_{tSL(L-1)}$, and the calculation formula is shown in (11) and (12).

$$\alpha_{rP(L-1)L} = \frac{A_{rP(L-1)}}{A_{iP(L-1)}} = \frac{1 - z_P}{1 + z_P} \tag{5}$$

$$\alpha_{rS(L-1)L} = \frac{A_{rS(L-1)}}{A_{iS(L-1)}} = \frac{1 - z_S}{1 + z_S} \tag{6}$$

$$\alpha_{tP(L-1)L} = \frac{A_{tPL}}{A_{iP(L-1)}} = \frac{2}{1 + z_P} \tag{7}$$

$$\alpha_{tS(L-1)L} = \frac{A_{tSL}}{A_{iS(L-1)}} = \frac{2}{1+z_S} \tag{8}$$

$$\alpha_{rPL(L-1)} = \frac{A_{tPL}}{A_{iPL}} = \frac{z_P-1}{1+z_P} \tag{9}$$

$$\alpha_{rSL(L-1)} = \frac{A_{rSL}}{A_{iSL}} = \frac{z_S-1}{1+z_S} \tag{10}$$

$$\alpha_{tPL(L-1)} = \frac{A_{tP(L-1)}}{A_{iPL}} = \frac{2z_P}{1+z_P} \tag{11}$$

$$\alpha_{tSL(L-1)} = \frac{A_{tS(L-1)}}{A_{iSL}} = \frac{2z_S}{1+z_S} \tag{12}$$

B. EQUIVALENT NODAL FORCE

Under the earthquake's action, the complex wave field of the layered foundation includes incident wave, reflected wave, refracted wave, and scattered wave. The incident wave, reflected wave, and refraction wave is free wave fields, and the viscous-spring artificial boundary absorbs the scattered wave field. The equivalent nodal force acting on the truncated boundary consists of two parts: one is the force required to overcome the stiffness and damping of the artificial boundary element; the other is the stress field of the free wave field at the artificial boundary:

$$F_b(t) = C_b\dot{u}_b(x_b, y_b, z_b, t) + K_b u_b(x_b, y_b, z_b, t) + \tau_b(x_b, y_b, z_b, t) \tag{13}$$

where F_b(t) is the equivalent nodal force of node b; $u_b(x_b, y_b, z_b, t)$ and $\dot{u}_b(x_b, y_b, z_b, t)$ denote the displacement and velocity at node b, respectively; $\tau_b(x_b, y_b, z_b, t)$ is the stress generated by the free wave field at node b; C_b and K_b are the spring stiffness and damping at node b, respectively; x_b, y_b and z_b are the coordinates of node b respectively

In the case of vertical incidence of seismic waves, the interface will not produce wave-type conversion, but due to the reflection and refraction of waves, the waves will stack in time sequence. In order to facilitate the calculation, the following assumptions are made for stratum and seismic wave: (1) The formation interface is parallel to the ground, that is, the horizontal interface; (2) The stratum is a layered infinite half-space elastic medium; (3) The medium in the layer is homogeneous and isotropic.

In this paper, the two-layer horizontal layered foundation is taken as an example to research. Fig. 4 shows the vertical propagation process of waves on a layered foundation. In order to show more clearly, the vertical propagating waves are drawn separately. The total wave number of the first layer is D and that of the second layer is U. The impedance of S- wave and P-wave in the first layer are $\rho_1 V_{S1}$ and $\rho_1 V_{P1}$, respectively, and the impedance of S-wave and P-wave in the second layer are, respectively, $\rho_2 V_{S2}$ and $\rho_2 V_{P2}$.

According to equations (5) - (12), the displacement and velocity amplitudes of different nodes are obtained at different times, and the equivalent nodal forces are determined at different times. Taking S-wave as an example, the formula of equivalent nodal forces of boundary nodes is deduced,

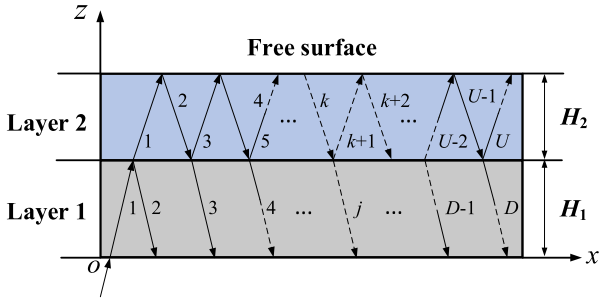

FIGURE 4. The vertical propagation process of elastic waves in the layered foundation.

the calculation formula of the first layer boundary as follows:

$$\begin{aligned} F_{bx1}^{-z} = {} & S_{b1}\{K_{T1}[u(t) + \alpha_{rS12}u(t-\Delta t_{rS1}) \\ & - \sum_{j=3}^{D}((\alpha_{rS21})^{j-3}\alpha_{tS12}\alpha_{tS21}u(t-\Delta t_{tS1}(j)))] \\ & + 2C_{T1}\dot{u}(t)\} \end{aligned} \tag{14}$$

$$\begin{aligned} F_{bx1}^{x} = {} & S_{b1}\{K_{N1}[u(t-\Delta t_{iS1}) + \alpha_{rS12}u(t-\Delta t_{rS1}) \\ & - \sum_{j=3}^{D}((\alpha_{rS21})^{j-3}\alpha_{tS12}\alpha_{tS21}u(t-\Delta t_{tS1}(j)))] \\ & + C_{N1}[\dot{u}(t-\Delta t_{iS1}) + \alpha_{rS12}\dot{u}(t-\Delta t_{rS1}) \\ & - \sum_{j=3}^{D}((\alpha_{rS21})^{j-3}\alpha_{tS12}\alpha_{tS21}\dot{u}(t-\Delta t_{tS1}(j)))\} \end{aligned} \tag{15}$$

$$\begin{aligned} F_{bz1}^{x} = {} & -S_{b1}\{C_{T1}[\dot{u}(t-\Delta t_{tS1}) - \alpha_{rS12}\dot{u}(t-\Delta t_{rS1}) \\ & - \sum_{j=3}^{D}((\alpha_{rS21})^{j-3}\alpha_{tS12}\alpha_{tS21}\dot{u}(t-\Delta t_{tS1}(j)))\} \end{aligned} \tag{16}$$

$$\begin{aligned} F_{bx1}^{-y} = {} & S_{b1}\{K_{T1}[u(t-\Delta t_{iS1}) + \alpha_{rS12}u(t-\Delta t_{rS1}) \\ & - \sum_{j=3}^{D}((\alpha_{rS21})^{j-3}\alpha_{tS12}\alpha_{tS21}u(t-\Delta t_{rS1}(j)))] \\ & + C_{T1}[\dot{u}(t-\Delta t_{iS1}) + \alpha_{rS12}\dot{u}(t-\Delta t_{rS1}) \\ & - \sum_{j=3}^{D}((\alpha_{rS21})^{j-3}\alpha_{tS12}\alpha_{tS21}\dot{u}(t-\Delta t_{rS1}(j)))\} \end{aligned} \tag{17}$$

$$F_{bx1}^{-x} = F_{bx1}^{x}; \quad F_{bz1}^{-x} = -F_{bz1}^{x}; \quad F_{bx1}^{y} = F_{bx1}^{-y} \tag{18}$$

$$\begin{aligned} F_{by1}^{-z} = {} & F_{bz1}^{-z} = F_{by1}^{x} = F_{by1}^{-x} = F_{by1}^{-y} = F_{bz1}^{-y} \\ = {} & F_{by1}^{y} = F_{bz1}^{y} = 0 \end{aligned} \tag{19}$$

The calculation formula of the second layer boundary as follows:

$$\begin{aligned} F_{bx2}^{x} = {} & S_{b2}\{K_{N2}[\sum_{k=1}^{U}((\alpha_{rS21})^{\varphi(k)}\alpha_{tS12}u(t-\Delta t_{rS2}(k)))] \\ & + C_{N2}[\sum_{k=1}^{U}((\alpha_{rS21})^{\varphi(k)}\alpha_{tS12}\dot{u}(t-\Delta t_{rS2}(k)))\} \end{aligned} \tag{20}$$

$$F_{bz2}^{x} = -S_{b2} \times \{C_{T2}[\sum_{k=1}^{U}((-1)^{k+1}(\alpha_{rS21})^{\varphi(k)}\alpha_{tS12}\dot{u}(t-\Delta t_{rS2}(k)))\}] \quad (21)$$

$$F_{bx2}^{-y} = S_{b2}\{K_{T2}[\sum_{k=1}^{U}((\alpha_{rS21})^{\varphi(k)}\alpha_{tS12}u(t-\Delta t_{rS2}(k)))] + C_{T2}[\sum_{k=1}^{U}((\alpha_{rS21})^{\varphi(k)}\alpha_{tS12}\dot{u}(t-\Delta t_{rS2}(k)))\}] \quad (22)$$

$$F_{bx2}^{-x} = F_{bx2}^{x}; \quad F_{bz2}^{-x} = -F_{bz2}^{x}; \quad F_{bx2}^{y} = F_{bx2}^{-y} \quad (23)$$

$$F_{by2}^{-z} = F_{bz2}^{-z} = F_{by2}^{x} = F_{by2}^{-x} = F_{by2}^{-y} = F_{bz2}^{-y} = F_{by2}^{y} = F_{bz2}^{y} = 0 \quad (24)$$

where the subscript of equivalent nodal force F denote the node number, the component direction of force, and the layer number, respectively, while the superscript represents the external normal direction of the side boundary where the node is located, which is positive when consistent with the coordinate axis direction, and negative on the contrary. u is S-wave and its vibration direction is x direction. Δt represents the time delay of the wave at point b, and the subscripts i, r, and t denote the incident wave, reflected wave, and transmitted wave, respectively; P and S represent P-wave and S-wave, respectively; 1 and 2 denote that the node is in the first layer and the node is in the second layer, respectively. Δt can be calculated by (25)–(28)

$$\Delta t_{iS1} = h/V_{S1} \quad (25)$$

$$\Delta t_{rS1} = (2H_1 - h)/V_{S1} \quad (26)$$

$$\Delta t_{tS1}(j) = \Delta t_{rS1} + 2H_2/V_{S2} \cdot (j-2) \quad (27)$$

$$\Delta t_{rS2}(k) = H_1/V_{S1} + (H_1 - h)/V_{S2} \cdot (-1)^k + 2H_2/V_{S2} \cdot (k - 0.5 + 0.5 \cdot (-1)^k) \quad (28)$$

where h is the distance from node b on the model boundary to the bottom boundary. H_1 and H_2 denote the height of the first and second layers of soil, respectively. j and k both denote function independent variables.

In (20)–(22), $\varphi(k)$ is an auxiliary function that can make the calculation more convenient, which can be calculated by (29)

$$\varphi(k) = (2k - 3 - (-1)^k)/4 \quad (29)$$

To apply the method proposed in this paper to engineering application, the corresponding seismic input program of the layered foundation is compiled to realize wave motion input.

IV. CALCULATION EXAMPLE OF TWO LAYER HORIZONTAL LAYERED FOUNDATION

A. LAYERED FOUNDATION MODEL

The finite element model is a two-layer foundation, as shown in Fig. 5. The model's size is 20 × 20 × 50m, and the height of the upper and lower floors are both 25m, and the origin of coordinates is o point. The model element is an 8-node hexahedron element with a mesh size of 1m × 1m × 1 m.

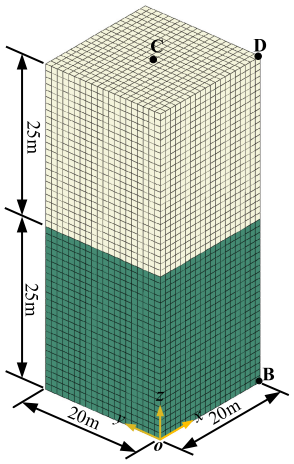

FIGURE 5. Three-dimensional layered finite element model.

Considering the size effect of the element, the element's size is carefully calculated to ensure that the high-frequency wave will not be filtered [17]. In order to facilitate the analysis and comparison, four monitoring points are selected on the model, namely point A (10m, 10m, 0), point B (20m, 0, 0), point C (10m, 10m, 50m), and point D (20m, 0, 50m). The upper and lower layers' density is both 200kg / m^3, Poisson's ratio is 0.25, the elastic modulus of the upper layer is 6Mpa, and the lower layer is 24MPa. In order to better compare the wave propagation law, the effect of foundation damping is not considered.

In order to compare the accuracy of the input method proposed in this paper, the theoretical solution is used as the reference solution. Two different input methods are set up: Method 1 is the traditional method, in which only the reflection of the wave at the top of each layer is considered; Method 2 is the method introduced in this article, in which all reflected and refracted waves in each layer is considered.

B. SIMPLE HARMONIC INPUT

It is assumed that a single period S-wave is input vertically from the bottom of the model in Fig. 5, and the displacement time history is shown in Fig. 6.

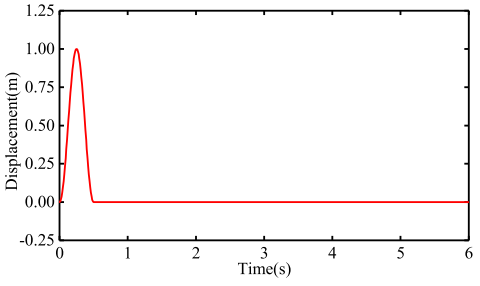

FIGURE 6. Input displacement time history.

1) COMPARISON OF DIFFERENT METHODS

Fig. 7 shows the displacement time histories of monitoring points A–D under two different harmonic input methods. According to the analysis in Fig. 7(a) and 7(b), each monitoring point's displacement time histories in method 1 are consistent with the bottom's theoretical value within 0–2.2s; the displacement time histories of each monitoring point in method 1 no longer fluctuates up and down in 2.2–6s, which is quite different from the theoretical solution at the bottom; in the whole time domain, the displacement time histories of each monitoring point in method 2 is consistent with the theoretical solution. According to the analysis in Fig. 7(c) and 7(d), each monitoring point's displacement time histories in method 1 is consistent with the theoretical value within 0–2.6s; the displacement time histories of each monitoring point in method 1 no longer fluctuate up and down in 2.6–6s, which is quite different from the bottom's theoretical solution; similarly, in the whole time domain, each monitoring point's displacement time histories in method 2 are consistent with the theoretical solution.

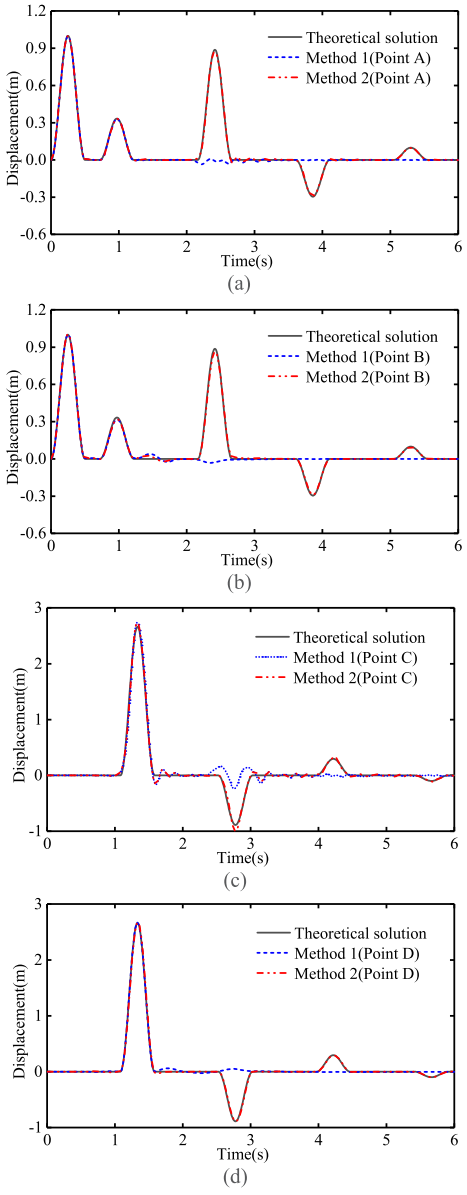

FIGURE 7. Displacement time histories of monitoring point A-D under two different simple harmonic input methods.

2) COMPARISON OF DIFFERENT POINTS

Fig. 8 shows the displacement time histories of monitoring points A-D under the simple harmonic input method 2. According to Fig. 8(a), the displacement time histories of the truncated boundary on the bottom of the layered foundation model is consistent with that of the center point of the bottom surface; from the analysis of Fig. 8(b), the displacement time histories of the truncated boundary on the top of the layered foundation model is consistent with that of the center point of the top surface. Methods 1 and 2 demonstrate that the layered ground motion input method proposed in this paper has high accuracy.

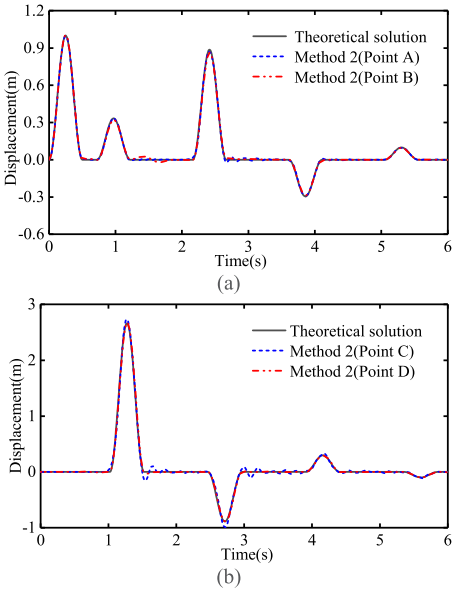

FIGURE 8. Displacement time histories of monitoring point A-D under harmonic input method 2.

C. SEISMIC WAVE INPUT

Example 1 verifies the input method's accuracy for layered ground motion when the harmonic wave is vertically input. To further verify the applicability of the proposed method in this paper, the Kobe seismic wave is selected to input vertically from the bottom of the model in Fig. 5, and the displacement time histories of each monitoring point of the model are analyzed. The seismic acceleration record of Kobe is shown in Fig. 9.

1) COMPARISON OF DIFFERENT METHODS

Fig. 10 shows the displacement response time histories of monitoring points A–D under two different seismic wave input methods. From the analysis in Fig. 10(a) and 10(b),

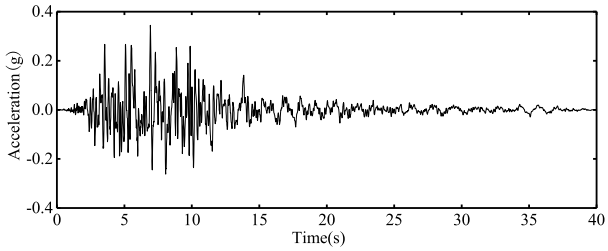

FIGURE 9. Kobe seismic acceleration dynamic record.

it can be seen that the displacement time histories law of each monitoring point in method 1 has large errors with the theoretical solution at the bottom; in the whole time domain, the displacement time histories of each monitoring point in method 2 is consistent with the theoretical solution at the bottom. From the analysis in Fig. 7(c) and 7(d), it can be seen that the amplitude and regularity of displacement time histories of each monitoring point in method 1 have large errors with the theoretical solution at the top; Similarly, in the whole time domain, the displacement time histories of each monitoring point in scheme 2 is consistent with the theoretical solution at the top.

2) COMPARISON OF DIFFERENT POINTS

Fig. 11 shows the displacement time histories of monitoring point A–D under seismic wave input method 2. It can be seen from Fig. 11 that the displacement time histories records of monitoring points A and B are highly consistent with the propagation law and numerical value of the theoretical solution at the top of the model. The displacement time histories records of monitoring points C and D are also highly consistent with the propagation law and numerical value of the theoretical solution at the top of the model.

Table 1 shows the comparison between the maximum and minimum values of monitoring points A-D in method 2 with the theoretical solution. It is shown from Table 1 that the relative error between the numerical solution and the theoretical solution is less than 5%, which fully shows that the numerical solution of this method has high accuracy.

TABLE 1. Comparison between the values of four monitoring points A-D and theoretical solutions.

Position	Max(m)	Error	Min(m)	Error
Theoretical solution	0.1104		-0.1001	
Point A	0.1100	0.36%	-0.0980	2.10%
Point B	0.1092	1.11%	-0.0956	4.51%
Theoretical solution	0.2412		-0.2041	
Point C	0.2420	0.34%	-0.2065	1.17%
Point D	0.2420	0.34%	-0.2050	0.44%

V. ENGINEERING EXAMPLE

Through the example in the third section, the accuracy of the proposed method is verified. An engineering example will further verify the accuracy of this method.

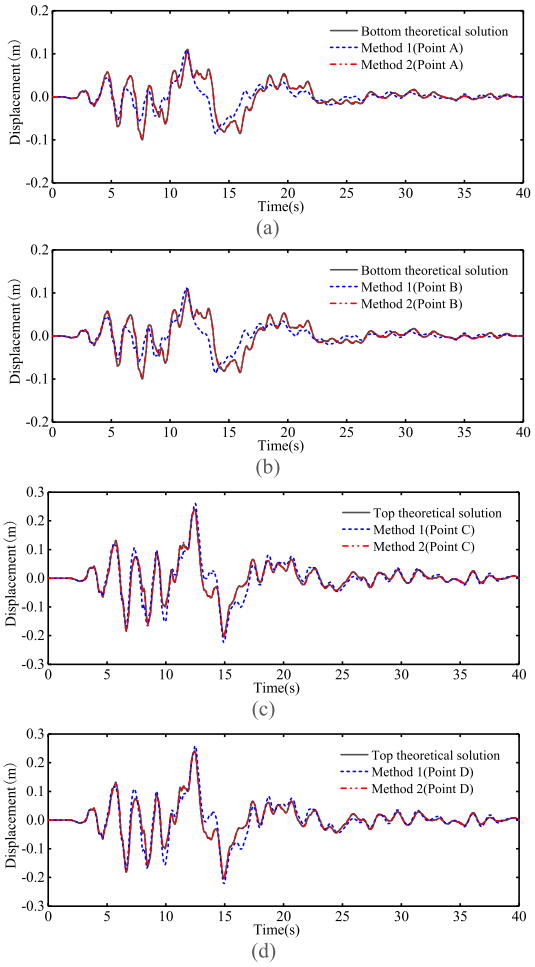

FIGURE 10. Displacement time histories of monitoring points A - D under two different seismic wave input methods.

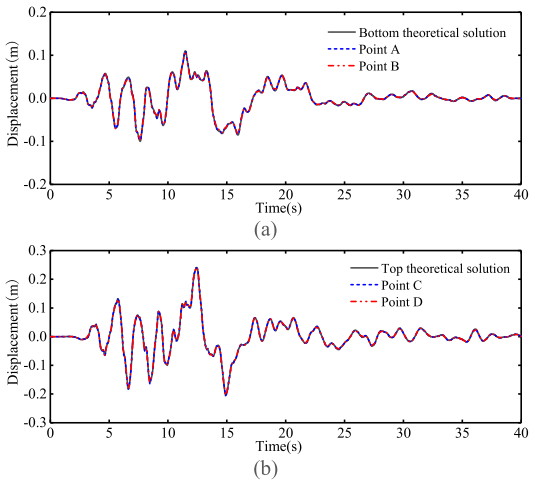

FIGURE 11. Displacement time histories curve of monitoring point A-D under seismic wave input method 2.

A. CALCULATION MODEL TWO-WAY SU RGE TOWER

The two-way surge tower is one of the essential hydraulic structures in the municipal water distribution project. It plays a role in water hammer protection to prevent water hammer

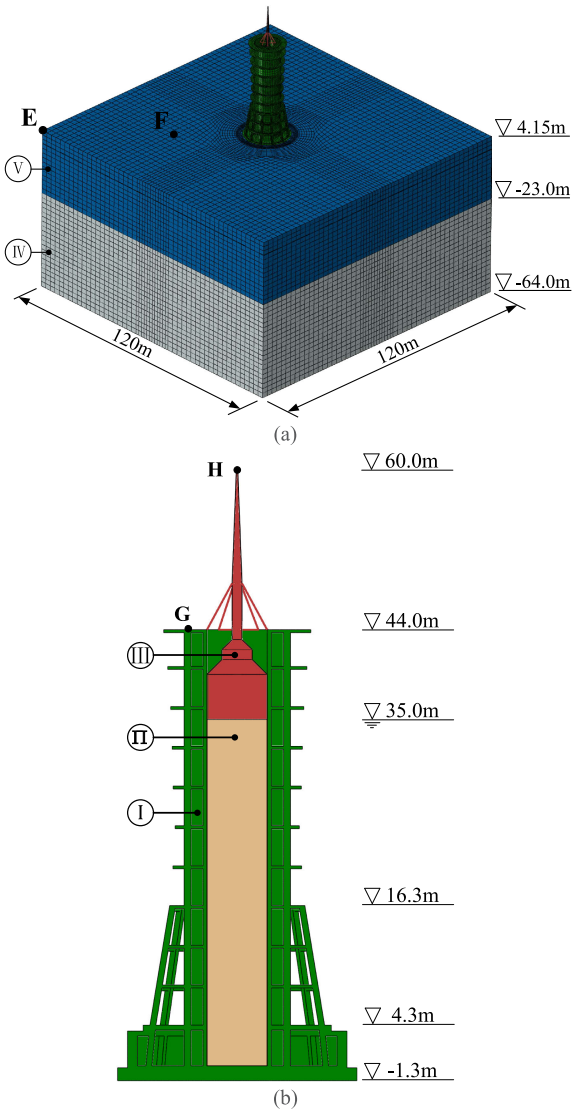

FIGURE 12. Integral calculation model of two-way surge tower (a) tower-foundation-water finite element model (b) tower finite element model.

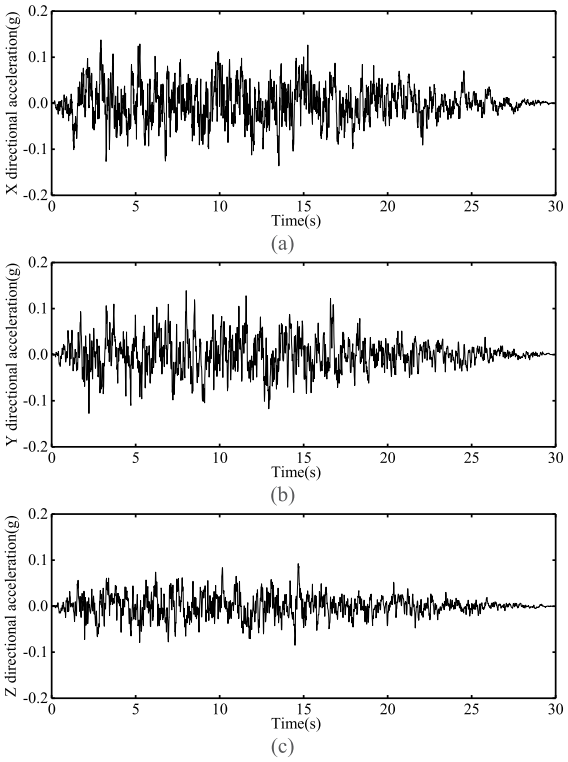

FIGURE 13. Three-dimensional ground motion records of the two-way surge tower.

pressure rise or pressure drop caused by a sudden change of velocity in the water delivery pressure pipeline to protect the pipeline system's safety.

The height of the two-way surge tower is 45.3m, and the building category is I grade. The project area is located in the sedimentary plain. Due to the sedimentary environment's continuous changes, the soil layer is unevenly distributed, and phase changes occur in the vertical direction, resulting in a more complex soil structure. C35 concrete is used for surge tower concrete, and Q235B killed steel is used for steel plates. The site elevation of the surge tower is 4.15m, the basement floor thickness is 1.50m, the lowest elevation of the bottom plate is −1.30m, the thickness of the roof is 0.5m, and the elevation of the top surface of the roof is 4.30m. The thickness of each floor of the surge tower above the ground is 0.30m. 43 C35 reinforced concrete cast-in-place piles with a diameter of 1.00m are arranged around the foundation under the surge tower's bottom plate. Among them, there are 19 long piles, the pile top elevation is −1.20m, the pile bottom elevation is −53.20m, the short pile is 24, the pile top elevation is −1.20m, and the pile bottom elevation is −33.20m. We intercept the finite foundation from the infinite foundation and combine the finite foundation and the tower to form an overall calculation model, as shown in Figure 12(a). The specific model of the tower is shown in Figure 12(b). In the dynamic calculation, a viscous-spring artificial boundary is applied to the finite foundation's truncated boundary to simulate the radiation damping effect of the infinite foundation, and equivalent nodal forces are applied to the truncated boundary to realize the ground motion input of the layered foundation.

According to the type of site, the time-domain non-stationary seismic wave is generated, as shown in Fig. 13. The horizontal direction's peak acceleration is 0.14g, and the acceleration in the vertical direction is 2 / 3 times that in the horizontal direction, which is 0.093g. For the convenience of comparison, two different input methods are adopted in this section. One is to consider only the reflection of the seismic wave at the top of each layer, such as waves 1 and 2 in Fig. 4; the other is to consider the full reflection and refraction process of seismic waves in each layer of foundation. In dynamic calculation, the dynamic elastic modulus of concrete needs to be 1.5 times the static elastic modulus [30].

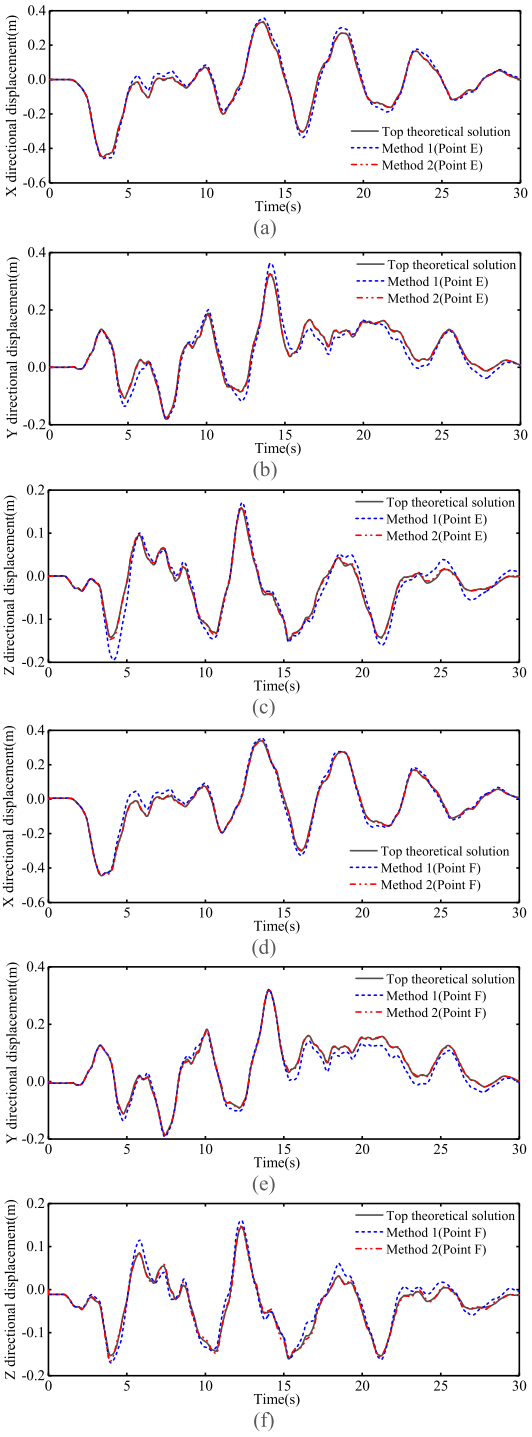

FIGURE 14. Three-dimensional displacement time histories seismic response of monitoring points E and F.

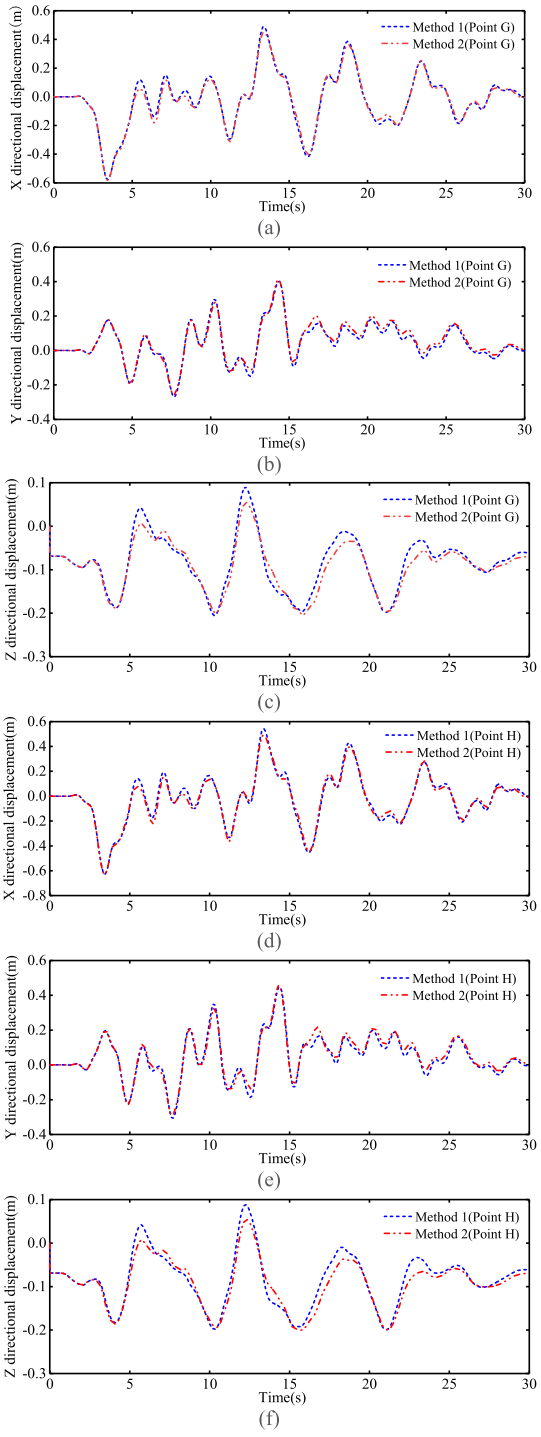

FIGURE 15. Three-dimensional displacement time histories seismic response of monitoring points G and H.

B. DYNAMIC RESPONSE OF TWO-WAY SURGE TOWER

1) DISPLACEMENT RESPONSE OF MONITORING POINTS ON FOUNDATION SURFACE

Fig. 14 shows the displacement time histories curves of monitoring points E and F on the foundation surface in three directions. It can be seen from Fig. 14 that the time histories curve of method 1 is quite different from the theoretical solution, and the time histories curve of method 2 is consistent with the theoretical solution. The example of the surge tower also shows that the proposed method has high accuracy.

2) DISPLACEMENT RESPONSE OF TOWER MONITORING POINTS

The three-dimensional displacement time histories curve of monitoring points G and H of the two-way surge tower is

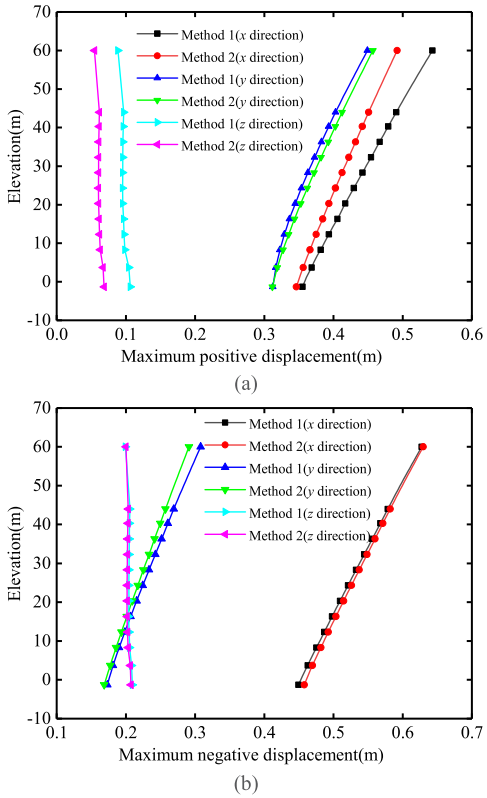

FIGURE 16. Maximum displacement response of two-way surge tower under three-dimensional earthquake action.

TABLE 2. Static material parameters of the model.

Materials	Density (kg/m^3)	Young's modulus(MPa)	Poisson's ratio
I(Concrete)	2500	31500.00	0.167
II(Water)	1000	2200.00	
III(Steel)	7850	210000.00	0.267
IV(Silty clay)	1915	13.54	0.290
V(Silty sand)	1830	25.40	0.320

shown in Fig. 15. It can be seen from Fig. 15 that there is a large error between method 1 and method 2, and the error in the vertical direction is the largest.

The maximum positive and maximum negative displacement response relationship of each node along the surge tower's elevation is shown in Fig. 16. As can be seen from Fig. 16 (a), the maximum displacement difference in positive x-direction of method 1 and method 2 increases with the increase of elevation, and the maximum displacement difference is 0.05m; the maximum displacement in the z-direction of method 2 is always 0.035m larger than that of method 1. It can be seen from Fig. 16 (b) that the maximum displacement difference in the positive y-direction of method 1 and method 2 increases with the increase of elevation, and the maximum displacement of method 1 is 0.017m larger than that of method 2.

Combined with the analysis of 16 (a) and 16 (b), the maximum displacement response of method 1 is larger than that of method 2.

VI. CONCLUSION

This paper establishes a viscous-spring artificial boundary model of layered foundations to simulate infinite foundations' radiation damping effect. The equivalent nodal force calculation formulas are derived from realizing the layered foundation's ground motion input based on the wave mechanics theory. First, a viscous-spring artificial boundary was applied to the two-layer horizontal finite foundation model's truncated boundary to simulate the two-layer infinite foundation's radiation damping effect, and equivalent nodal forces were applied on the truncated boundary, which verified the accuracy and effectiveness of the method. It is then applied to the layered foundation-tower-water dynamic interaction. The ground motion input method proposed in this paper is compared with the traditional ground motion input method. The results show that: (1) Through the calculation results of the two-layer horizontal finite foundation calculation example, the dynamic displacement response of the top point C and the bottom point A of the model is higher consistent with the theoretical solution. The dynamics displacement of the points (B and D) of the truncated boundary and the nodes on the same surface is consistent. These altogether demonstrate that the viscous-spring artificial boundary model and ground motion input method in this paper has higher accuracy and better stability. (2) The overall system of layered foundation-tower-water applies the method in this paper. According to the dynamic calculation results, the dynamic displacement responses of points E and F on the foundation's upper surface are consistent with the theoretical solution. Compared with the method in this paper, the dynamic displacement response of the points E and F of the tower calculated by the traditional method is larger. When analyzing the dynamic interaction of the horizontally layered foundation-tower-water system, the ground motion input method proposed in this paper has higher calculation accuracy.

The models and methods presented in this paper are only applicable to horizontally layered foundations. However, in practice, the site soil may exist with laterally heterogeneous mediums. In this case, the elastic wave will undergo a waveform transformation at the interface of the medium. The methods cannot use in in laterally heterogeneous soil. Therefore, we will conduct further research on the ground motion input method of inclined layered foundation. Besides, structural characteristics, foundation types, soil stiffness, frequency content, duration and intensity of ground motion, and other parameters on the structural response of layered foundation will also be the focus of our research.

REFERENCES

[1] Y. Li, T. Bao, J. Gong, X. Shu, and K. Zhang, "The prediction of dam displacement time series using STL, extra-trees, and stacked LSTM neural network," *IEEE Access*, vol. 8, pp. 594440–594452, 2020, doi: 10.1109/access.2020.2995592.

[2] L. Jingbo and L. Yandong, "A direct method for analysis of dynamic soil-structure interaction based on interface idea," *Develop. Geotechn. Eng.*, vol. 83, no. 3, pp. 261–276, Dec. 1998, doi: 10.1016/s0165-1250(98)80018-7.

[3] A. K. Chopra and P. Chakrabarti, "Earthquake analysis of concrete gravity dams including dam-water-foundation rock interaction," *Earthq. Eng. Struct. Dyn.*, vol. 9, no. 4, pp. 363–383, Jan. 1981, doi: 10.1002/eqe.4290090406.

[4] H. Y. Zhang, L. J. Zhang, H. J. Wang, and C. N. Guan, "Influences of the duration and frequency content of ground motions on the seismic performance of high-rise intake towers," *Eng. Failure Anal.*, vol. 91, pp. 481–495, Sep. 2018, doi: 10.1016/j.engfailanal.2018.04.039.

[5] P. E. Kavitha, K. S. Beena, and K. P. Narayanan, "A review on soil–structure interaction analysis of laterally loaded piles," *Innov. Infrastruct. Solutions*, vol. 1, no. 1, pp. 1–14, Dec. 2016, doi: 10.1007/s41062-016-0015-x.

[6] H. Lan, J. Liu, and Z. Bai, "Wave-field simulation in VTI media irregular free surface," *Chin. J. Geophys. Chin. Ed.*, vol. 54, no. 8, pp. 2072–2084, Aug. 2011, doi: 10.3969/j.issn.0001-5733.2011.08.014.

[7] M. K. Kim, Y. M. Lim, and W. Y. Cho, "Three dimensional dynamic response of surface foundation on layered half-space," *Eng. Struct.*, vol. 23, no. 11, pp. 1427–1436, Nov. 2011, doi: 10.1016/S0141-0296(01)00051-7.

[8] Q. Liang, "Summary and review of the numerical methods for analyzing soil-structure dynamic interaction," *J. Bejing Jiaotong Univ.*, vol. 21, no. 6, pp. 690–694, Dec. 1997.

[9] C. Liao, X.-M. Zhong, J. Fang, and W. Chen, "A local absorbing boundary condition based on the one-way wave equations," in *Proc. IEEE Antennas Propag. Soc. Int. Symp.*, Albuquerque, NM, USA, Jul. 2006, pp. 2731–2734, doi: 10.1109/APS.2006.1711168.

[10] A. J. Deeks and M. F. Randolph, "Axisymmetric time-domain transmitting boundaries," *J. Eng. Mech.*, vol. 120, no. 1, pp. 25–42, Jan. 1994, doi: 10.1061/(ASCE)0733-9399(1994)120:1(25).

[11] J. Liu, Y. Du, X. Du, Z. Wang, and J. Wu, "3D viscous-spring artificial boundary in time domain," *Earthq. Eng. Eng. Vib.*, vol. 5, no. 1, pp. 93–102, Jun. 2006, doi: 10.1007/s11803-006-0585-2.

[12] X. Du and M. Zhao, "A local time-domain transmitting boundary for simulating cylindrical elastic wave propagation in infinite media," *Soil. Dyn. Earthq. Eng.*, vol. 30, no. 10, pp. 937–946, Oct. 2010, doi: 10.1016/j.soildyn.2010.04.004.

[13] L. Chen and L. J. Zhang, "Seismic response of gravity dam under oblique incidence of seismic waves," *Adv. Mater. Res.*, vols. 838–841, pp. 1585–1590, Nov. 2013, doi: 10.4028/www.scientific.net/AMR.838-841.1585.

[14] Y. Gao, Y. Xu, and F. Jin, "The dynamic analysis of gravity dam-layered foundation interaction based on a high-order doubly asymptotic open boundary," *Chin. J. Geophys.*, vol. 62, no. 7, pp. 2582–2590, Nov. 2019.

[15] J. P. Wolf and M. Preisig, "Dynamic stiffness of foundation embedded in layered halfspace based on wave propagation in cones," *Earthq. Eng. Struct. Dyn.*, vol. 32, no. 7, pp. 1075–1098, Jun. 2003, doi: 10.1002/eqe.263.

[16] N. Nakamura, "A practical method for estimating dynamic soil stiffness on surface of multi-layered soil," *Earthq. Eng. Struct. Dyn.*, vol. 34, no. 11, pp. 1391–1406, Sep. 2005, doi: 10.1002/eqe.487.

[17] C. Birk and R. Behnke, "A modified scaled boundary finite element method for three-dimensional dynamic soil-structure interaction in layered soil," *Int. J. Numer. Methods Eng.*, vol. 89, no. 3, pp. 371–402, Jan. 2012, doi: 10.1002/nme.3251.

[18] L.-M. Fan and L.-Y. Zhang, "Time-history algorithm for earthquake effect in layered-soil site," *Rock Soil Mech.*, vol. 30, no. 9, pp. 2564–2568, Sep. 2009.

[19] J. Liang, J. Fu, and Z. Ba, "The effect of dynamic characteristics of layered half-space on soil-structure interaction," in *Proc. Int. Conf. Electr. Technol. Civil Eng. (ICETCE)*, Lushan, China, Apr. 2011, pp. 4621–4624, doi: 10.1109/ICETCE.2011.5775436.

[20] Z. Han, G. Lin, and H. Zhong, "Modified scaled boundary finite element method solution for dynamic stiffness matrix of laminar foundation," *Water Resour. Power.*, vol. 30, no. 7, pp. 100–104, Jul. 2012.

[21] X. Chen, C. Bibk, and C. Song, "Transient analysis of wave propagation in layered soil by using the scaled boundary finite element method," *Comput. Geotech.*, vol. 63, pp. 1–12, Jan. 2015, doi: 10.1016/j.compgeo.2014.08.008.

[22] S. Prempramote, C. Song, F. Tin-Loi, and G. Lin, "High-order doubly asymptotic open boundaries for scalar wave equation," *Int. J. Numer. Methods Eng.*, vol. 79, no. 3, pp. 340–374, Jul. 2009, doi: 10.1002/nme.2562.

[23] Y. Gao, C. Song, F. Jin, and Y. Xu, "A simplified high order doubly asymptotic open boundary for modeling elastic wave propagation in layered foundation," *Scientia Sinica Technol.*, vol. 46, no. 5, pp. 527–534, May 2016, doi: 10.1360/N092015-00175.

[24] T. Liu, S. Zheng, X. Tang, and Y. Gao, "Time-domain analysis of underground station-layered soil interaction based on high-order doubly asymptotic transmitting boundary," *Comput. Model. Eng. Sci.*, vol. 120, no. 3, pp. 545–560, Jan. 2019, doi: 10.32604/cmes.2019.05043.

[25] G. Yin, L. Zhao, and T. Li, "Viscoelastic artificial boundary model considering layered foundation," *Adv. Sci. Technol. Water Resour.*, vol. 39, no. 3, pp. 87–94, May 2019, doi: 10.3880/j.issn.1006-7647.2019.03.015.

[26] P. Sotoudeh, M. Ghaemian, and H. Mohammadnezhad, "Seismic analysis of reservoir-gravity dam-massed layered foundation system due to vertically propagating earthquake," *Soil Dyn. Earthq. Eng.*, vol. 116, pp. 174–184, Jan. 2019, doi: 10.1016/j.soildyn.2018.09.041.

[27] L. Chen and L. Zhang, "Study on obliquely incident seismic waves based on viscous-spring boundary," *J. Hydroelectr. Eng.*, vol. 34, no. 1, pp. 183–188, Jan. 2015.

[28] H. Xu, X. Du, M. Zhao, and J. Wang, "Effect of oblique incidence of seismic waves on seismic responses of high arch dam," *J. Hydroelectr. Eng.*, vol. 30, no. 6, pp. 159–165, Dec. 2011.

[29] T. Łodygowski and W. Sumelka, "Limitations in application of finite element method in acoustic numerical simulation," *J. Theor. Appl. Mech.*, vol. 44, no. 4, pp. 849–865, Jun. 2006.

[30] Y. Zhai, Z. Bi, Y. Tang, and T. Ma, "Study on damage and failure of gravity dam under main aftershock sequence based on NGA model," *J. Hydraulic Eng.*, vol. 51, no. 2, pp. 152–157, Feb. 2020.

ZHONGHUI BI received the B.S. degree in water resources and hydropower engineering from the Hefei University of Technology, Hefei, China, in 2014. He is currently pursuing the M.S. degree in hydraulic structural engineering with Hohai University. His research interests include seismic research of hydraulic structures, seismic input methods, and artificial synthetic seismic wave algorithm.

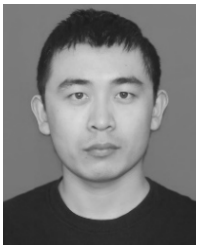

BINGHUI CUI received the B.S. and M.S. degrees in civil engineering from the Anhui University of Science and Technology, Huainan, China, in 2013 and 2016, respectively. He is currently pursuing the Ph.D. degree in disaster prevention mitigation and protection engineering with Hohai University. His research interests include application smoothed particle hydrodynamics for simulating landslide and seismic research of hydraulic structures.

YAFEI ZHAI received the B.S. degree in water resources and hydropower engineering from the North China University of Water Resources and Electric Power, Zhengzhou, China, in 2014, and the M.S. degree, in 2017. He is currently pursuing the Ph.D. degree in hydraulic structural engineering with Hohai University. His research interest includes seismic research of hydraulic structures.